ChemPhysChem

Research Article
doi.org/10.1002/cphc.202300975

Chemistry Europe
European Chemical Societies Publishing

www.chemphyschem.org

Online-Monitoring of the Enantiomeric Ratio in Microfluidic Chip Reactors Using Chiral Selector Ion Vibrational Spectroscopy

Sonja Schmahl,[a] Francine Horn,[a, b] Jiaye Jin,[a] Hannes Westphal,[c] Detlev Belder,[c] and Knut R. Asmis*[a]

A novel experimental approach for the rapid online monitoring of the enantiomeric ratio of chiral analytes in solution is presented. The charged analyte is transferred to the gas phase by electrospray. Diastereomeric complexes are formed with a volatile chiral selector in a buffer-gas-filled ion guide held at room temperature, mass-selected, and subsequently spectrally differentiated by cryogenic ion trap vibrational spectroscopy. Based on the spectra of the pure complexes in a small diastereomer-specific spectral range, the composition of diastereomeric mixtures is characterized using the cosine similarity score, from which the enantiomeric ratio in the solution is determined. The method is demonstrated for acidified alanine solutions and using three different chiral selectors (2-butanol, 1-phenylethanol, 1-amino-2-propanol). Among these, 2-butanol is the best choice as a selector for protonated alanine, also because the formation ratio of the corresponding diastereomeric complexes is found to be independent of the nature of the enantiomer. Subsequently, a microfluidic chip is implemented to mix enantiomerically pure alanine solutions continuously and determine the enantiomeric ratio online with minimal sample consumption within one minute and with competitive accuracy.

Introduction

Molecular chirality plays a central role in how the building blocks of life, like amino acids, sugars, or nucleotides, interact. Since the handedness of drugs, agrochemicals, and flavors can be crucial for their effects and efficiency, chirality analysis is of fundamental importance.[1] For this purpose, various methods have been developed and established, among them circular dichroism, nuclear magnetic resonance, and, most commonly, chromatography with chirality-selective columns.[2] However, these methods are often associated with high sample consumption, low sensitivity, and time-expensive steps.

A reduction in sample and time consumption can be achieved by downscaling the analysis to the micrometer level.[3] Microfluidic chips can serve as continuous-flow microreactors for studying chemical conversions at minimum residence times far from equilibrium, integrating reaction and simultaneous analysis on a single device. This enables the development of lab-on-a-chip systems, facilitating automated screening of enantioselective reactions, while reaction conditions can be optimized under the perspective of increased yields and enantioselectivity.[4] Analysis can be performed either on the chip, keeping the analytes in solution, or it can be decoupled from the reaction solution by transferring the analytes into the gas phase.

The significant interest in highly sensitive and fast chirality analysis has resulted in the development of powerful gas-phase methods for distinguishing enantiomers, determining enantiomeric ratios, characterizing the absolute configuration, and understanding chirality recognition, in general.[5] Most of these methods are based on the formation of diastereomers e.g. by the addition of a chiral selector in solution. Thereby, homo- and heterochiral diastereomers are formed, depending on whether analyte and selector have the same or different handedness. They can be distinguished based on energetic and/or structural aspects. Jet-cooled neutral complexes have been studied using various techniques, mainly with electronic, vibrational, and rotational spectroscopy.[6] Particularly, the development of microwave three-wave mixing and chiral tag rotational spectroscopy has enabled new opportunities in chirality analysis, including the determination of the absolute configuration.[7] The sensitivity of these methods is limited, making it challenging to investigate ionic species, due to their lower number density in the gas phase.[8]

Mass spectrometric (MS) methods generally require ions for the chirality analysis of mass-selected species.[9,10] Diastereomeric ionic complexes can be distinguished based on their thermodynamic or kinetic stability,[11] dissociation rates probed by either collision-induced dissociation (CID),[12] infrared[13] or

[a] S. Schmahl, F. Horn, Dr. J. Jin, Prof. Dr. K. R. Asmis
Wilhelm-Ostwald-Institut für Physikalische und Theoretische Chemie, Universität Leipzig, Linnéstraße 2, 04103 Leipzig (Germany)
E-mail: knut.asmis@uni-leipzig.de

[b] F. Horn
Fritz-Haber-Institut der Max-Planck-Gesellschaft, Faradayweg 4–6, 14195 Berlin (Germany)

[c] H. Westphal, Prof. Dr. D. Belder
Institut für Analytische Chemie, Universität Leipzig, Linnéstraße 3, 04103 Leipzig (Germany)

Supporting information for this article is available on the WWW under https://doi.org/10.1002/cphc.202300975

ultraviolet photodissociation,[14] or different effective collision cross sections in ion mobility spectrometry (IMS).[15] However, these methods often rely on energy differences between the diastereomers and the interpretation of complex fragmentation patterns can be demanding. IMS for enantiomer-specific analysis is currently limited by the resolution required to resolve diastereomers since the difference in the corresponding collision cross sections is typically small. The data reproducibility when using chiral drift gas modifiers is still under discussion.[16]

Infrared photodissociation (IRPD) spectroscopy is attracting growing attention as a tool for chirality analysis of mass-selected ions.[13] IRPD spectroscopy can distinguish between diastereomeric complexes and provides spectral and structural information that facilitates understanding of chirality recognition. Early chirality-sensitive experiments explored the structures of proteins as well as small peptides bound to metal ions.[17] Filippi *et al.* investigated diastereomeric complexes between calixarene derivatives and nucleosides.[18] The chirality recognition of amino acids by cyclodextrins was intensively studied.[19] Another approach is the examination of homo- and heterochiral dimers of enantiomers. Klyne *et al.* probed the chirality recognition of protonated glutamic acid dimers.[20] Recently, the structures of various amino acid dimers and dipeptides were analyzed with IRPD spectroscopy.[21] Furthermore, multimers, such as the serine octamer and its derivatives, have been the subject of numerous investigations.[22] Another recent field is the analysis of diastereomeric glycans utilizing IRPD spectroscopy.[23]

While IRPD spectroscopy has been used to study chirality recognition, no determination of enantiomeric ratios has been performed using this technique. Here, we present an experimental procedure where a chiral selector is added to the ionic chiral analyte in the gas phase, to decouple chirality analysis from solution phase chemistry. The method requires the use of enantiomerically pure, volatile chiral selectors to form diastereomeric complexes with the ionic analytes. In a proof-of-principle experiment, complexes between protonated alanine (chiral analyte) and *S*-2-butanol (chiral selector) are investigated using cryogenic ion trap vibrational spectroscopy.[24] Spectral differences in the IRPD spectra of these ion/molecule complexes are exploited to measure the diastereomeric ratio in the gas phase, from which the enantiomeric ratio present in the solution can be determined. For this purpose, a microfluidic chip, used for mixing the enantiomerically pure analyte solutions and continuous sampling of the mixtures, is coupled to a cryogenic ion trap triple mass spectrometer. In addition, two other chiral selectors, *S*-1-phenylethanol and *R*-1-amino-2-propanol, are tested for their applicability in differentiating alanine enantiomers.

Experimental Section

Cryogenic Ion Trap Vibrational Spectroscopy

IRPD experiments were performed using the 6 K ion-trap triple mass spectrometer described previously.[24,26] The experimental procedure conducted in these experiments is schematically presented in Figure 1. Briefly, protonated alanine ions are transferred solvent- and fragment-free to the gas phase from a 10 mmol/L solution of D- or L-alanine in 1:1 methanol to water with 0.1 % formic acid using a custom-built nanospray ion source or a microfluidic chip reactor. The ions are then thermalized and the beam of ions is collimated in a first, He-buffer-gas-filled radio frequency (RF) octupole ion guide. A steady flow of the volatile chiral selector (*S*-2-butanol, *S*-1-phenylethanol, or *R*-1-amino-2-propanol) seeded in He (≤ 2 %) exits the top mouth of a Stefan-tube-like reservoir into the second RF octupole ion guide, also held at room temperature. Ion-molecule complexes between protonated alanine and the selector are formed and stabilized by many collisions with the carrier gas. The ionic diastereomeric complexes are mass-selected using a quadrupole mass filter and guided into

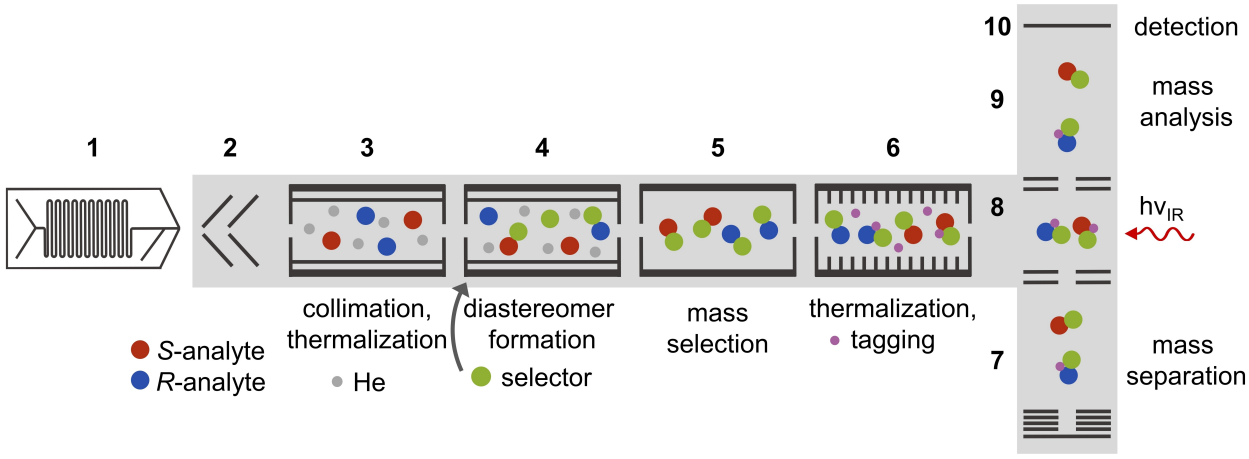

Figure 1. Schematic representation of the experimental procedure. (1) Analyte ions are transferred from a microfluidic chip into vacuum by electrospray. (2) After passing two skimmers, (3) the ions are collimated and thermalized in a first He-filled RF ion guide. (4) The volatile, neutral chiral selector is introduced to the second RF ion guide, where diastereomeric complexes are formed by three-body collisions. (5) The diastereomers are mass-selected with a quadrupole mass filter and focused into an RF ring-electrode ion trap. (6) Here, ions are thermalized to cryogenic temperatures and messenger-tagged. Ions are extracted into an orthogonally mounted reflectron time-of-flight (TOF) mass spectrometer, where they are (7) reflected by 180°. Messenger-tagged ions are refocused at the center of the extraction region, where they (8) interact with IR radiation. Ions and photofragments are reaccelerated into the (9) field-free region of the TOF, which allows (10) background-free detection with a microchannel plate detector.[25]

an RF ring-electrode ion trap. The trap, filled with deuterium (D_2) as a buffer gas, was held at a nominal temperature of 12 K. Here, the ions are thermalized and weakly bound ion-messenger complexes with D_2 are formed.[27]

IRPD spectra are obtained using the background-free IR^1MS^2 measurement scheme.[25] Every 100 ms all ions are extracted from the ion trap and focused into the center of the extraction region of an orthogonally mounted reflectron time-of-flight (TOF) tandem photofragmentation mass spectrometer. Ions are accelerated in the direction of the reflectron, where they are reflected by 180°, refocused at the center of the extraction region, and subsequently reaccelerated to allow background-free photofragment detection. Photofragments are obtained by irradiating the ions with tunable IR radiation from a Nd:YAG laser (Continuum Surelight EX1) pumped OPO/OPA/$AgGaSe_2$ laser system (Laser Vision) operated at 10 Hz and with a bandwidth of approximately 3.5 cm^{-1}.[28] IRPD spectra are recorded by continuously scanning the laser wavelength, which is monitored online (HighFinesse WS6-600 wavelength meter), with a scan speed, such that a TOF mass spectrum averaged over 20 laser shots is obtained every 2 cm^{-1}. For experiments conducted to determine enantiomeric ratios a smaller scan speed is used, such that a TOF mass spectrum averaged over 20 laser shots is obtained every 1 cm^{-1}. Typically, three to four scans are measured and averaged to obtain an IRPD spectrum. The photodissociation cross section σ_{IRPD} is determined as described previously.[24,26]

Microfluidic Chip Reactor

The full-body glass chip (Borofloat 33; dimensions: 22 mm length, 10 mm width, 2 mm depth) used for the present experiments was manufactured by IX-factory (now: Micronit, Dortmund, Germany; the design was a modification of a previous version). After manufacturing, a monolithic pyramidal nano-electrospray emitter was ground at the reactor outlet and subsequently hydrophobized.[29] Generally, the chip can be used as a microreactor or for mixing different compounds and enables direct electrospray MS-hyphenation for online detection. The two front inlets were used for introducing analyte solutions by syringe pumps (Nemesys low-pressure pumps, Cetoni, DE). A subsequent meander structure ensures rapid homogeneous mixing. Past the mixing structure, an additional fluidic inlet is integrated for the addition of further reagents (e.g. formic acid for improving the ion yield in the electrospray process). This inlet was furthermore used for electrical contact for electrospray ionization via a stainless-steel union (360 μm, 100 μm bore, VICI AG, Schenkon, Switzerland). All other connections were realized by commercially available PEEK and FS tubing and fittings (360 μm outer diameter, 75–100 μm inner diameter). The connections to the chip inlets were realized by custom-made steel clamps, which enable low dead-volume connection of the tubing directly to the chip channels. A picture of the chip and the IRPD-hyphenation can be found in Figure S1.

Online Preparation of Enantiomeric Mixtures

For the online preparation of enantiomeric mixtures, the nanospray ion source was replaced by the microfluidic chip described above. 10 mmol/L solutions of D- and L-alanine in 1:1 methanol to water were mixed in the chip channels. The total flow rate was 0.6 μL/min. The relative flow rates of the two channels containing the enantiomerically pure solutions were varied to adjust the ratio between the two enantiomers. Ions were sprayed by applying a voltage of 3.5 kV to a 0.1 % solution of formic acid in 1:1 methanol to water pumped in the sheath channel with a flow rate of 0.4 μL/min.

Cosine Similarity Score

To obtain an objective measure for the agreement between two experimental spectra, the cosine similarity score *CSS* was employed.[25,30] The score expresses the similarity between two spectra, which are condensed and represented by two n-dimensional vectors, **A** and **B**. The cosine of the angle θ between the two vectors is calculated using their normalized Euclidean dot product according to:

$$CSS = cos(\theta) = \frac{\boldsymbol{A} \cdot \boldsymbol{B}}{\|\boldsymbol{A}\|\|\boldsymbol{B}\|} = \frac{\sum_{i=1}^{n} A_i B_i}{\sqrt{\sum_{i=1}^{n} A_i^2}\sqrt{\sum_{i=1}^{n} B_i^2}}. \quad (1)$$

Here, a score closer to unity indicates greater similarity.

Enantiomeric Ratio Determination

The relative ratios of mixtures can also be determined using the *CSS*, whenever the IRPD spectra of two known compositions (e.g. pure compounds) are available. The spectrum of a mixture $Spect_{mix}$ of homo- and heterochiral complexes can be written as the linear combination of the spectra of its pure constituents $Spect_{homo}$ and $Spect_{hetero}$:

$$Spect_{mix} = x_{homo} Spect_{homo} + (1 - x_{homo}) Spect_{hetero}. \quad (2)$$

Here, the fraction of the heterochiral complex is given by $x_{hetero} = (1 - x_{homo})$. A Nelder-Mead downhill simplex algorithm[31] is used to maximize the *CSS* of the experimentally obtained spectrum with the spectrum calculated according to Equation 2, $CSS = Spect_{expt} \cdot Spect_{mix}$ by varying the fraction of the homochiral complex x_{homo}. The convergence criterion of the *CSS* is 0.001.

To correlate the diastereomeric ratio with the enantiomeric ratio in solution and to account for deviations in the gas-phase formation of the homo- and heterochiral complexes from the enantiomeric fractions x_L and x_D, respectively, two proportional constants c_{homo} and c_{hetero} are defined, which are not known a priori. For the *S*-enantiomer of the chiral selector, the fraction of the homochiral complex x_{homo} can then be written as:

$$x_{homo} = \frac{c_{homo} x_L}{c_{homo} x_L + c_{hetero}(1 - x_L)} = \frac{x_L}{x_L + r(1 - x_L)}, \quad (3)$$

with $r = \frac{c_{hetero}}{c_{homo}}$, the gas phase formation ratio of the homo- and heterochiral complexes.

Material

S-2-butanol (Arcos Organics, 99 %), *S*-1-phenylethanol (Arcos Organics, 99 %), *R*-1-Amino-2-propanol (Arcos Organics, ≥ 98 %), D-alanine (Sigma-Aldrich, ≥ 99 %), L-alanine (Sigma-Aldrich, ≥ 99 %), and methanol (Sigma-Aldrich, ≥ 99.9 %) were used without further purification.

Results and Discussion

Mass Spectrometry

Figure 2 displays the quadrupole mass spectrum obtained by spraying an acidic alanine (Ala) solution and introducing 2-butanol (2-BuOH) in the second RF octupole ion guide. Under

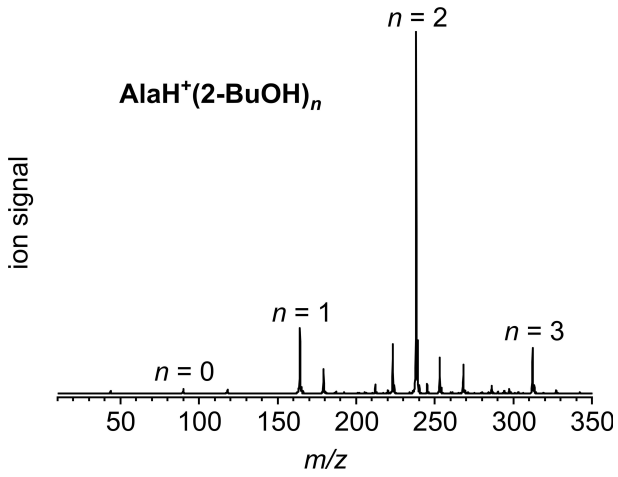

Figure 2. Quadrupole mass spectrum obtained by spraying a 10 mmol/L solution of alanine in 1:1 water to methanol with 0.1% formic acid and introducing a gas mixture of 1–2% 2-butanol in He (chamber pressure: ~$2\cdot10^{-4}$ mbar) in the second RF octupole ion guide held at room temperature. Ion optics settings were optimized for a maximum ion yield at *m/z* 238 ($n=2$).

these conditions protonated alanine/2-butanol complexes, $AlaH^+(2\text{-}BuOH)_n$, with up to three 2-butanol ligands (*m/z* 164, *m/z* 238, *m/z* 312) are formed. The smaller peaks correspond to other ions formed in the process, such as $Ala_{1\text{-}3}H^+$ (*m/z* 90, *m/z* 179, *m/z* 268) and $(2\text{-}BuOH)_3H^+$ (*m/z* 223).

The formation of $AlaH^+(2\text{-}BuOH)_n$ complexes with $n \leq 3$ is very efficient. However, it is not possible to distinguish between homo- and heterochiral complexes or even to determine their fraction based on their mass-to-charge ratio. This requires additional information, which can be obtained by recording IRPD spectra of the mass-selected diastereomers.

IRPD Spectroscopy

The mass-selected diastereomeric complexes $AlaH^+(2\text{-}BuOH)_n$ were D_2-messenger-tagged in the ring-electrode trap with a tagging efficiency of roughly 60%. IRPD spectra were subsequently obtained using the background-free MS^2IR^1 measurement scheme.[25] Figure 3 compares the spectrum of the D_2-tagged $AlaH^+$ to those of the D_2-tagged homo- and heterochiral complexes of $AlaH^+(2\text{-}BuOH)_n$ with $n=1$–3.

Based on the previous assignment by Fischer *et al.*[32] of the IRPD spectrum of D_2-tagged $AlaH^+$, the spectra shown in Figure 3 are divided into three regions, each attributed to a particular type of vibrational transition. OH stretching bands of the alanine carboxyl group and the 2-butanol hydroxy group appear in the range from 3700 to 3450 cm^{-1} (A). Free NH stretching modes of the alanine amino group are observed in the range from 3450 to 3100 cm^{-1} (B). Hydrogen-bonded NH stretching bands typically appear as broader peaks in the range from 3100 to 2200 cm^{-1} (C),[33] thus overlapping with CH stretching bands around 2900 cm^{-1}. The peak positions in the spectral regions A and B are summarized in Table S1.

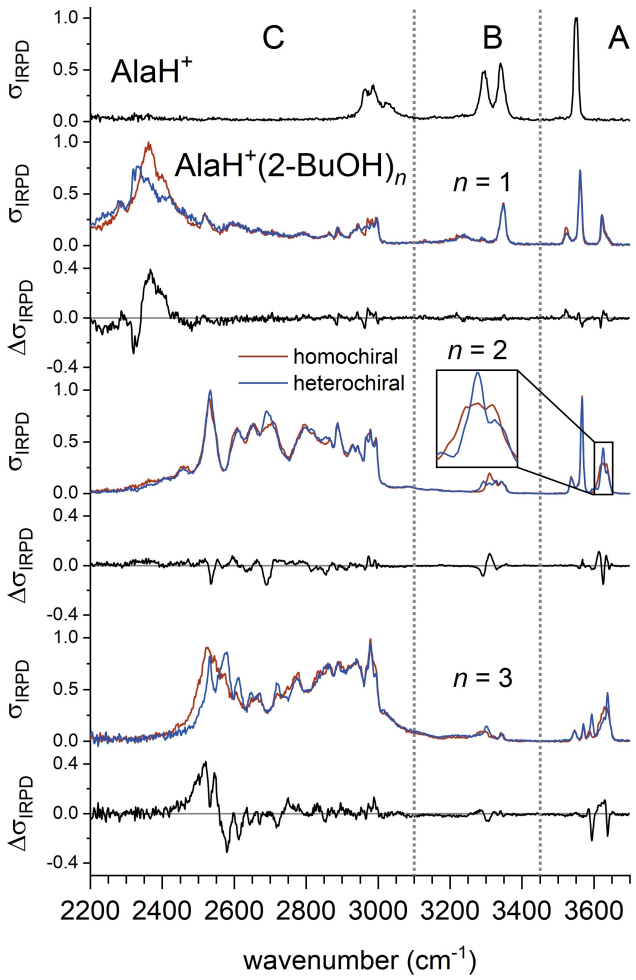

Figure 3. IRPD spectrum of D_2-tagged $AlaH^+$ in comparison to D_2-tagged $AlaH^+(2\text{-}BuOH)_n$ complexes in the spectral range from 3700 to 2200 cm^{-1}. The spectra of the homo- and heterochiral complexes are shown in red and blue, respectively together with the related difference spectra in black. Dashed lines separate regions characteristic of the excitations of OH stretching (A), free NH stretching (B), CH stretching, and hydrogen-bonded NH stretching modes (C).

Even though the exact knowledge of the structure of the diastereomeric complexes is not needed for the evaluation of the enantiomeric ratio, we briefly summarize here, what structural information can be directly extracted from the IRPD spectra of $AlaH^+(2\text{-}BuOH)_n$ with $n=1$–3 shown in Figure 3. The strong IR activity in region C in all spectra together with a decrease of the IR activity in region B reveals that complex formation takes place via hydrogen bonding between the amino group of protonated alanine and the hydroxy group of 2-butanol. Hydrogen bonds with the carboxyl group can be excluded up to $n=2$, since the free carboxylic OH stretching mode at 3550 cm^{-1} in the spectrum of $AlaH^+$ (upper trace in Figure 3) remains unaffected upon the addition of the first two 2-butanol ligands. The third 2-butanol does bind to the acid group, leaving one free NH group.

Similarities and differences of the IRPD spectra of the respective homo- and heterochiral complexes are discussed in more detail as these are required for the analysis of enantio-

meric ratios. This can be evaluated by calculating the *CSS* for each set of spectra for certain regions.[25,30] The score is expressed as a percentage. The smaller the value, the greater the differences between the two experimental spectra. The values obtained for the spectra shown in Figure 3 for the entire spectral range as well as for the individual regions A to C are listed in Table 1.

Inspection of the *CSS* values obtained for $AlaH^+(2\text{-BuOH})_n$ reveals that the spectral differences are, indeed, quite small, but quantifiable and that they markedly depend on the number of selector molecules *n*. The largest differences, considering the entire spectral range probed in these experiments, are found for the set of spectra with $n=1$ (*CSS* = 96.4%). Smaller *CSS* values are found for the individual regions A to C and, interestingly, each complex exhibits a different characteristic region, i.e., for $n=1$ the lowest *CSS* value is found for region C (*CSS* = 96.2%), while for $n=2$ and $n=3$, the lowest *CSS* values are obtained for region B (*CSS* = 91.6%) and A (*CSS* = 91.2%), respectively. Therefore, the overall difference of the spectra may decrease as the number of selectors increases, but at a particular spectral region, the relative differences may actually be more pronounced for larger *n*. This needs to be considered when defining fast and reliable measurement protocols for the determination of the enantiomeric ratio (see below).

Comparison With Other Chiral Selectors

Besides *S*-2-butanol, two other volatile chiral substances, *S*-1-phenylethanol (1-PhEtOH) and *R*-1-amino-2-propanol (MIPA), were tested for the differentiation of alanine enantiomers. All chosen selectors are able to form hydrogen bonds with either the alanine amino group or the acid group. However, the number of ligands that effectively form diastereomeric complexes varies, as can be seen from the mass spectra in Figures S2 and S3. In contrast to three 2-butanol ligands, only two 1-phenylethanol ligands bind to protonated alanine at room temperature under similar experimental conditions. This is attributed to the steric hindrance of the bulky phenyl group. 1-amino-2-propanol offers another binding site due to the additional amino group. This allows the formation of larger complexes with up to five 1-amino-2-propanol ligands.

IRPD spectra of homo- and heterochiral complexes of $AlaH^+(1\text{-PhEtOH})_n$ and $AlaH^+(MIPA)_n$ are shown in Figure 4. The spectra of $AlaH^+(1\text{-PhEtOH})_n$ with $n=1$–2 show strong IR activity in region C, similar to $AlaH^+(2\text{-BuOH})_n$, indicating hydrogen bonding between the amino group of protonated alanine and the hydroxy group of 1-phenylethanol. The spectra of $AlaH^+(MIPA)_n$ with $n=1$–3 are more different from the spectra of the other two alanine/selector complexes due to the additional amino group in 1-amino-2-propanol. Again, strong IR activity in region C is observed in all spectra, indicating hydrogen bonding with amino groups. In the spectra of the complexes with $n=1$ the OH stretching band of the carboxyl group at 3550 cm^{-1}, observed for $AlaH^+$ is no longer present. Therefore, complex formation most likely occurs via hydrogen bonding between the carboxyl group of protonated alanine and the amino group of 1-amino-2-propanol. Whether the second and third ligand binds directly to the amino acid or the amino group of another 1-amino-2-propanol is difficult to determine from the IRPD spectra alone. An indication of the latter is that the spectra of the diastereomers are not noticeably different from each other, as is the case with the other two selectors.

Binding to another 1-amino-2-propanol is less sensitive towards the stereochemistry of the analyte than binding to it directly. This becomes apparent when the cosine similarity of the spectra of the respective homo- and heterochiral complexes of $AlaH^+(MIPA)_n$ with $n=1$–3 are calculated. The *CSS* is greater than 99%, both over the entire range and in the individual regions A, B, and C for all sets of spectra. Therefore, 1-amino-2-propanol is not suitable for the differentiation of alanine enantiomers. Also, no substantial spectral differences can be identified for $AlaH^+(1\text{-PhEtOH})_n$ with $n=1$. In contrast, $AlaH^+(1\text{-PhEtOH})_n$ with $n=2$ exhibits the largest differences, considering the entire spectral range probed in these experiments (*CSS* = 95.0%). However, the formation of $AlaH^+(1\text{-PhEtOH})_n$ is experimentally more challenging because of the low vapor pressure

Table 1. Cosine similarity score *CSS* (in percent) for diastereomeric complexes of $AlaH^+(2\text{-BuOH})_n$, $AlaH^+(1\text{-PhEtOH})_n$, and $AlaH^+(MIPA)_n$ in the given spectral regions (in cm^{-1}).

spectral range (cm^{-1})		3700–2200[a]	3700–3450	3450–3100	3100–2200[a]
region		A + B + C	A	B	C
complex				*CSS* (%)	
$AlaH^+(2\text{-BuOH})_n$	$n=1$	96.4	98.8	99.3	96.2
	$n=2$	99.5	98.3	91.6	99.7
	$n=3$	97.7	91.2	96.3	97.9
$AlaH^+(1\text{-PhEtOH})_n$	$n=1$	99.5	99.4	99.3	99.6
	$n=2$	95.0	95.0	65.4	96.5
$AlaH^+(MIPA)_n$	$n=1$	99.8	99.9	99.8	99.8
	$n=2$	99.9	99.9	99.9	99.9
	$n=3$	99.8	97.7	99.7	99.6

[a] For $AlaH^+(1\text{-PhEtOH})_n$ the range from 3700(3100)–2400 cm^{-1} was considered.

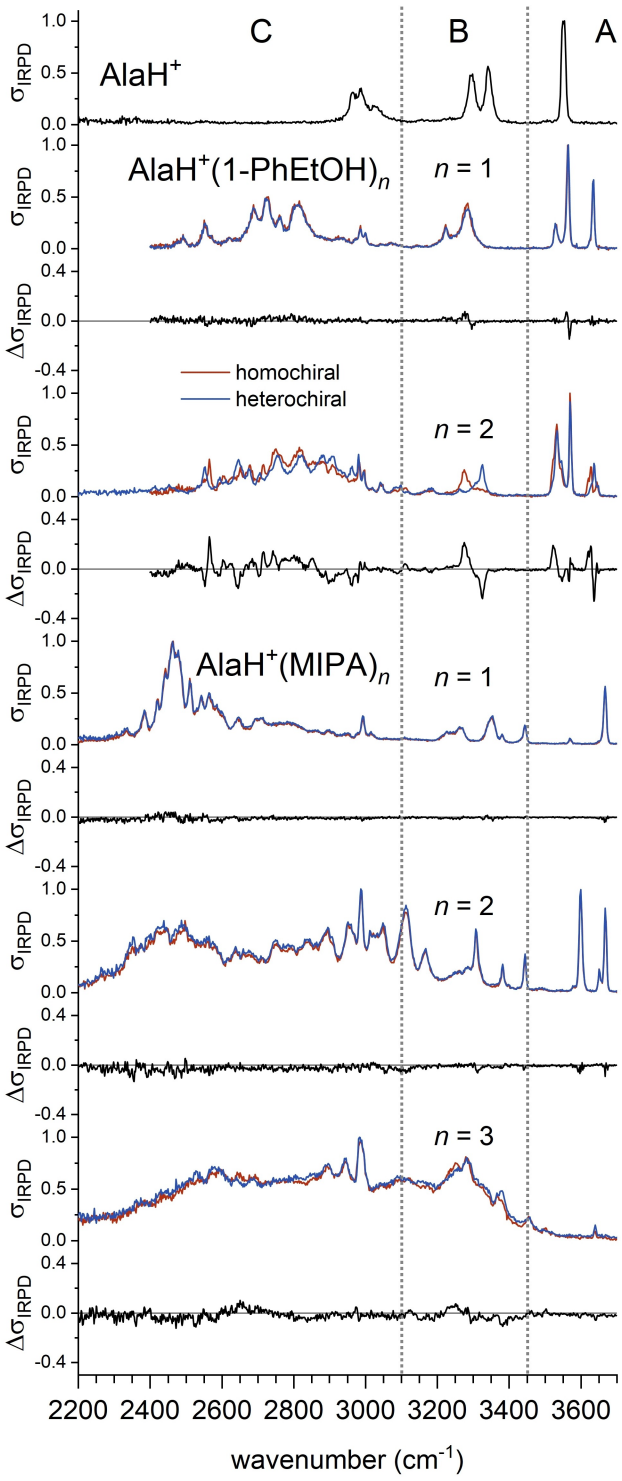

Figure 4. IRPD spectrum of D_2-tagged $AlaH^+$ in comparison to D_2-tagged $AlaH^+(1\text{-PhEtOH})_n$ and $AlaH^+(MIPA)_n$ complexes in the spectral range from 3700 to 2200 cm^{-1}. The spectra of the homo- and heterochiral complexes are shown in red and blue, respectively together with the related difference spectra in black. Dashed lines separate regions characteristic of the excitation of OH stretching (A), free NH stretching (B), CH stretching, and hydrogen-bonded NH stretching modes (C).

of 1-phenylethanol (0.1 hPa at 20 °C) compared to the vapor pressure of 2-butanol (16.5 hPa at 20 °C) leading to lower ion intensities for $AlaH^+(1\text{-PhEtOH})_n$ and the formation of water adducts that may overlap with the ions of interest, as can be seen in Figure S2. Therefore, 2-butanol remains the best choice as a selector for protonated alanine among those investigated here.

Determination of Enantiomeric Ratios

The IRPD spectra can be used to quantify the relative composition of mixtures. An IRPD spectrum of a mixture can be represented as a linear combination of the spectra of its components, here, the pure homo- and heterochiral complexes. From the spectrum of the mixture, the fraction x_{homo} of the homochiral complexes, and thus the diastereomeric ratio, can be extracted. This is done by calculating sum spectra of the single-component spectra as a function of x_{homo} according to equation 2 and comparing them to the spectrum of the (unknown) mixture by calculating the cosine similarity score *CSS*. Maximizing *CSS* by optimizing x_{homo} will give the combination that best reflects the spectrum of the mixture. The procedure is exemplarily depicted in Figure S4.

Recording the IRPD spectra across larger spectral regions is time-consuming and not necessary as there is little or no diastereomer-specific information in most areas. Therefore, it is advantageous to limit the experiment to a small spectral range with significant differences. Additionally, a high parent ion yield and a large IRPD cross section are advantageous, as this reduces the signal-to-noise ratio. The highest ion yield was obtained for the $AlaH^+(2\text{-BuOH})_n$ complexes with $n=2$ (see Figure 2). To find the most suitable spectral range for these complexes, we calculated *CSS* for spectral intervals of 30 cm^{-1} of the spectra of $AlaH^+(2\text{-BuOH})_2$, as shown in Figure S5. Only intervals containing IRPD cross-sections larger than 15% of the maximum cross-section were considered. Therefore, region B was excluded from the analysis, even though it exhibits the smallest *CSS* in this spectrum. The *CSS* values for intervals in region C are too close to 100% for the approach. A closer look into the results for region A reveals, that the range from 3640 to 3610 cm^{-1} contains highly diastereomer-specific information (*CSS* = 94.2%). We therefore limit the scanning range to this part of the spectrum to minimize the measurement time. For better comparison, the single-component spectra were rerecorded prior to the analysis of mixtures to ensure that all measurements were performed under the same conditions.

To investigate how the diastereomeric ratio correlates with the enantiomeric ratio in solution, enantiomerically pure solutions of D- and L-alanine are mixed on a microfluidic chip. The enantiomeric ratio is then tuned by adjusting the relative flow rates $Q_L/(Q_L+Q_D)$ and $Q_D/(Q_L+Q_D)$ of the enantiomeric-pure solutions, while the total flow rate Q_L+Q_D is kept constant. The fraction x_{homo} (in percent) of the homochiral complex L-$AlaH^+(S\text{-2-BuOH})_2$ is determined as described above and compared to the relative flow rate $Q_L/(Q_L+Q_D)$ (in percent) and therefore the fraction x_L of L-alanine in solution. To determine the precision of the method, ten consecutive measurements

were performed for each molar ratio. The results are shown in Figure 5. All values can be found in Table S2.

A fit according to equation 3 results in a formation ratio $r = 1.000$ with a correlation coefficient $R^2 = 0.999$. The average absolute deviation of x_{homo} from the relative flow rate is $\pm 1.1\,\%$ and the maximum absolute deviation is 2.4%. The standard deviation, indicated by the error bars in Figure 5, is below 3.5% for all measurements.

The experiment was repeated using distinct mixtures of D- and L-alanine solutions, each with another mixing ratio, sprayed with the nanospray source (see Figure S6 and Table S3). The results closely resemble those achieved with the microfluidic chip. We can conclude that the use of the chip doesn't introduce additional errors that need to be considered. Additionally, this illustrates the method's reproducibility.

A formation ratio of 1.000 indicates that c_{homo} and c_{hetero} are identical and formation energy differences of the diastereomeric complexes investigated in this study are negligible and have no influence on the result within the uncertainty of the measurement. The diastereomeric ratio in the gas phase is equal to the enantiomeric ratio in solution. This is in agreement with low- and high-energy gas-phase collision experiments between amino acids and 2-butanol that have found that the complex formation yield is independent of the stereochemistry of the colliding partners.[34] 2-Butanol has only one hydroxy group available for hydrogen bond formation and is a small conformationally flexible chiral molecule without any additional functional group. In combination with the small and less flexible chiral amino acid alanine, it is likely that the diastereomers exhibit minor but sufficient differences for spectral differentiation. However, they do not differ much in geometry and are energetically similar. Other systems may show a preference for the formation of a particular diastereomer, requiring calibration (e.g. using a racemic mixture) for analytical applications. Note that in most other mass spectrometric chirality analysis approaches, an energy difference between the diastereomers is a prerequisite for the differentiation of the two.[9]

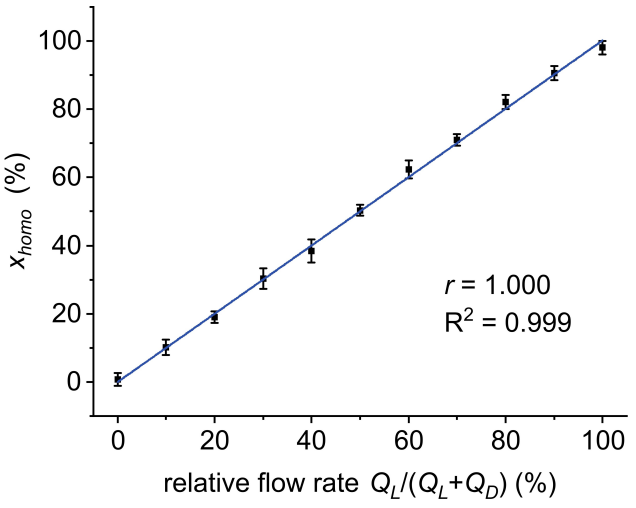

Figure 5. Calculated fraction x_{homo} in % of L-AlaH$^+$(*S*-2-BuOH)$_2$ plotted vs. the relative flow rate $Q_L/(Q_L+Q_D)$ of L-alanine in %. The line indicates a fit according to equation 3 and the error bars are the standard deviation of ten consecutive measurements.

Another aspect to consider is the coexistence of multiple isomers of a diastereomeric complex. The peaks above 3600 cm^{-1} in the spectra of homo- and heterochiral AlaH$^+$(2-BuOH)$_2$ indicate the presence of more than one isomer of both diastereomers. However, this does not impact the determination of the enantiomeric ratios, since the proportion of different isomers of one diastereomer remains unchanged under constant measurement conditions.

An enantiomerically pure analyte sample is preferable for obtaining the spectra of pure homo- and heterochiral complexes. Note that only one configuration is needed since the selector is typically available in both enantiomerically pure forms. However, if this is not the case, the spectra can likely be extracted from spectra with different enantiomeric ratios of the sample or the selector using factor analysis.[35] While the samples analyzed here were pure (except for impurities in the commercial sample), the method may be applicable to mixtures, such as reaction solutions, as long as there is no other ion with the same *m/z*. In addition, the performance of the method is independent of relative concentrations of analyte and selector.

The analysis of reactions without purification is facilitated by the addition of the selector in the gas phase, instead of in the solution, as in most of the MS-based methods for chiral analysis. This has several advantages. Enantiomeric ions are transferred to the gas phase with the same efficiency, which is not necessarily the case for diastereomers. Isolated enantiomeric intermediates, which are short-lived in solution, are stable in the gas phase and hence may be accessible for gas phase diastereomer formation followed by chirality analysis.[25] Furthermore, the selector cannot interfere with a chemical reaction. Adding the chiral selector directly to the reaction solution changes the reaction conditions, in the worst case, leading to side reactions of the selector with reactants.

With a measurement time of approximately one minute per scan, the method is competitive with chromatographic methods for the chirality analysis of alanine samples.[36] The accuracy is sufficient for many applications.

Conclusions

We have introduced a method for the fast and accurate determination of enantiomeric ratios of protonated alanine in microfluidic chip reactors based on differences in the IRPD spectra of diastereomeric, hydrogen-bonded complexes formed in the gas phase with a chiral selector. Given the ubiquity of hydrogen-bond interactions, the method holds promise to be adapted to the online monitoring of enantiomeric ratios of related systems, be it chiral reactants, products, or even transient intermediates.[25] More generally speaking, this method represents an important step towards automatically monitoring, adjusting, and optimizing reaction parameters of asymmetric reactions in real-time, to maximize selectivity and

product yield, while minimizing both sample consumption and sampling time.

Acknowledgments

This study was supported by the European Social Fund (ESF). J.J. acknowledges the Alexander von Humboldt-Stiftung for a postdoctoral fellowship. Open Access funding enabled and organized by Projekt DEAL.

Conflict of Interests

There are no conflicts to declare.

Data Availability Statement

The data that support the findings of this study are available from the corresponding author upon reasonable request.

Keywords: Chirality · Microreactors · Vibrational spectroscopy · Mass spectrometry · Hydrogen bonds

[1] E. Sanganyado, Z. Lu, Q. Fu, D. Schlenk, J. Gan, *Water Res.* **2017**, *124*, 527.
[2] a) P. L. Polavarapu (Ed.) *Chiral Analysis. Advances in Spectroscopy, Chromatography and Emerging Methods*, Elsevier, Amsterdam, Netherlands, **2018**; b) T. J. Wenzel, *Differentiation of Chiral Compounds Using NMR Spectroscopy*, John Wiley & Sons, Inc., Hoboken, NJ, USA, **2018**; c) G. K. E. Scriba (Ed.) *Chiral Separations. Methods and Protocols*, Humana Press, Totowa, NJ, USA, **2013**.
[3] A. J. DeMello, *Nature* **2006**, *442*, 394.
[4] a) N. Lu, J. P. Kutter, *Electrophoresis* **2020**, *41*, 2122; b) K. A. Kochetkov, N. A. Bystrova, P. A. Pavlov, M. S. Oshchepkov, A. S. Oshchepkov, *J. Ind. Eng. Chem.* **2022**, *115*, 62; c) S. Nagl, P. Schulze, S. Ohla, R. Beyreiss, L. Gitlin, D. Belder, *Anal. Chem.* **2011**, *83*, 3232.
[5] A. Zehnacker, *Chiral Recognition in the Gas Phase*, Taylor & Francis, Boca Raton, FL, USA, **2010**.
[6] A. Zehnacker, M. A. Suhm, *Angew. Chem. Int. Ed.* **2008**, *47*, 6970.
[7] a) S. R. Domingos, C. Pérez, M. D. Marshall, H. O. Leung, M. Schnell, *Chem. Sci.* **2020**, *11*, 10863; b) W. Sun, M. Schnell, *J. Phys. Chem. Lett.* **2023**, *14*, 7389; c) R. E. Sonstrom, Z. P. Vang, H. N. Scolati, J. L. Neill, B. H. Pate, J. R. Clark, *Org. Process Res. Dev.* **2023**, *27*, 1185; d) H. Singh, F. E. L. Berggötz, W. Sun, M. Schnell, *Angew. Chem. Int. Ed.* **2023**, *62*, e202219045.
[8] O. Asvany, S. Schlemmer, *Phys. Chem. Chem. Phys.* **2021**, *23*, 26602.
[9] D.-Q. Han, Z.-P. Yao, *TrAC Trends Anal. Chem.* **2020**, *123*, 115763.
[10] a) X. Chen, Y. Kang, S. Zeng, *Chirality* **2018**, *30*, 609; b) X. Yu, Z.-P. Yao, *Anal. Chim. Acta* **2017**, *968*, 1; c) H. Awad, A. El-Aneed, *Mass Spectrom. Rev.* **2013**, *32*, 466; d) L. Wu, F. G. Vogt, *J. Pharm. Biomed. Anal.* **2012**, *69*, 133.
[11] I. H. Chu, D. V. Dearden, J. S. Bradshaw, P. Huszthy, R. M. Izatt, *J. Am. Chem. Soc.* **1993**, *115*, 4318.
[12] a) W. A. Tao, R. G. Cooks, *Anal. Chem.* **2003**, *75*, 25 A–31 A; b) L. Wu, R. G. Cooks, *Anal. Chem.* **2003**, *75*, 678; c) Z.-P. Yao, T. S. M. Wan, K.-P. Kwong, C.-T. Che, *Anal. Chem.* **2000**, *72*, 5394; d) Z.-P. Yao, T. S. M. Wan, K.-P. Kwong, C.-T. Che, *Anal. Chem.* **2000**, *72*, 5383; e) K. A. Schug, W. Lindner, *J. Am. Soc. Mass Spectrom.* **2005**, *16*, 825.
[13] Y. Shi, M. Du, J. Ren, K. Zhang, Y. Xu, X. Kong, *Molecules* **2020**, *25*, 5152.
[14] a) D. Scuderi, P. Maître, F. Rondino, K. Le Barbu-Debus, V. Lepère, A. Zehnacker-Rentien, *J. Phys. Chem. A* **2010**, *114*, 3306; b) A. Fujihara, N. Maeda, T. N. Doan, S. Hayakawa, *J. Am. Soc. Mass Spectrom.* **2017**, *28*, 224; c) Y. Shi, M. Zhou, K. Zhang, L. Ma, X. Kong, *J. Am. Soc. Mass Spectrom.* **2019**, *30*, 2297.
[15] a) V. Domalain, M. Hubert-Roux, V. Tognetti, L. Joubert, C. M. Lange, J. Rouden, C. Afonso, *Chem. Sci.* **2014**, *5*, 3234; b) J. R. Enders, J. A. Mclean, *Chirality* **2009**, *21*, E253–E264.
[16] a) P. Dwivedi, C. Wu, L. M. Matz, B. H. Clowers, W. F. Siems, H. H. Hill, *Anal. Chem.* **2006**, *78*, 8200; b) R. Fernandez-Maestre, M. Doerr, *Anal. Methods* **2022**, *14*, 3011; c) H. H. Hill, *Anal. Chem.* **2022**, *94*, 3020.
[17] a) R. C. Dunbar, J. D. Steill, J. Oomens, *J. Am. Chem. Soc.* **2011**, *133*, 1212; b) Y. M. E. Fung, T. Besson, J. Lemaire, P. Maitre, R. A. Zubarev, *Angew. Chem. Int. Ed.* **2009**, *121*, 8490.
[18] a) A. Filippi, C. Fraschetti, S. Piccirillo, F. Rondino, B. Botta, I. D'Acquarica, A. Calcaterra, M. Speranza, *Chemistry* **2012**, *18*, 8320; b) F. Rondino, A. Ciavardini, M. Satta, A. Paladini, C. Fraschetti, A. Filippi, B. Botta, A. Calcaterra, M. Speranza, A. Giardini et al., *Rend. Fis. Acc. Lincei* **2013**, *24*, 259.
[19] a) S.-S. Lee, S. Park, Y. Hong, J.-U. Lee, J.-H. Kim, D. Yoon, X. Kong, S. Lee, H. B. Oh, *Phys. Chem. Chem. Phys.* **2017**, *19*, 14729; b) S.-S. Lee, J.-U. Lee, J. H. Oh, S. Park, Y. Hong, B. K. Min, H. H. L. Lee, H. I. Kim, X. Kong, S. Lee et al., *Phys. Chem. Chem. Phys.* **2018**, *20*, 30428; c) K. Hirata, Y. Mori, S.-I. Ishiuchi, M. Fujii, A. Zehnacker, *Phys. Chem. Chem. Phys.* **2020**, *22*, 24887; d) L. Sun, F. Huang, W. Liu, L. Lin, Y. Hong, X. Kong, *Spectrochim. Acta Part A* **2020**, *241*, 118653.
[20] J. Klyne, A. Bouchet, S.-I. Ishiuchi, M. Fujii, M. Schneider, C. Baldauf, O. Dopfer, *Phys. Chem. Chem. Phys.* **2018**, *20*, 28452.
[21] a) Å. Andersson, M. Poline, M. Kodambattil, O. Rebrov, E. Loire, P. Maître, V. Zhaunerchyk, *J. Phys. Chem. A* **2020**, *124*, 2408; b) Å. Andersson, M. Poline, K. J. Houthuijs, R. E. van Outersterp, G. Berden, J. Oomens, V. Zhaunerchyk, *J. Phys. Chem. A* **2021**, *125*, 7449; c) H. Wang, M. Heger, M. H. Al-Jabiri, Y. Xu, *Molecules* **2022**, *27*, 38; d) K. Yoshizawa, K. Hirata, S.-I. Ishiuchi, M. Fujii, A. Zehnacker, *ChemPhysChem* **2023**, *24*, e202300172.
[22] a) F. X. Sunahori, G. Yang, E. N. Kitova, J. S. Klassen, Y. Xu, *Phys. Chem. Chem. Phys.* **2013**, *15*, 1873; b) G. Liao, Y. Yang, X. Kong, *Phys. Chem. Chem. Phys.* **2014**, *16*, 1554; c) J. Ren, Y.-Y. Wang, R.-X. Feng, X.-L. Kong, *Chin. Chem. Lett.* **2017**, *28*, 537.
[23] a) E. Mucha, A. Stuckmann, M. Marianski, W. B. Struwe, G. Meijer, K. Pagel, *Chem. Sci.* **2019**, *10*, 1272; b) C. J. Gray, I. Compagnon, S. L. Flitsch, *Curr. Opin. Struct. Biol.* **2020**, *62*, 121.
[24] N. Heine, K. R. Asmis, *Int. Rev. Phys. Chem.* **2015**, *34*, 1.
[25] M. Mayer, K. R. Asmis, *J. Phys. Chem. A* **2021**, *125*, 2801.
[26] N. Heine, K. R. Asmis, *Int. Rev. Phys. Chem.* **2016**, *35*, 507.
[27] M. Brümmer, C. Kaposta, G. Santambrogio, K. R. Asmis, *J. Chem. Phys.* **2003**, *119*, 12700.
[28] W. R. Bosenberg, D. R. Guyer, *J. Opt. Soc. Am. B* **1993**, *10*, 1716.
[29] H. Westphal, R. Warias, C. Weise, D. Ragno, H. Becker, M. Spanka, A. Massi, R. Gläser, C. Schneider, D. Belder, *React. Chem. Eng.* **2022**, *7*, 1936.
[30] L. J. M. Kempkes, J. Martens, G. Berden, K. J. Houthuijs, J. Oomens, *Faraday Discuss.* **2019**, *217*, 434.
[31] J. A. Nelder, R. Mead, *Comput. J.* **1965**, *7*, 308.
[32] K. C. Fischer, S. L. Sherman, J. M. Voss, J. Zhou, E. Garand, *J. Phys. Chem. A* **2019**, *123*, 3355.
[33] a) E. G. Diken, N. I. Hammer, M. A. Johnson, R. A. Christie, K. D. Jordan, *J. Chem. Phys.* **2005**, *123*, 164309; b) P. J. Kelleher, C. J. Johnson, J. A. Fournier, M. A. Johnson, A. B. McCoy, *J. Phys. Chem. A* **2015**, *119*, 4170.
[34] a) K. Kulyk, O. Rebrov, M. Ryding, R. D. Thomas, E. Uggerud, M. Larsson, *J. Am. Soc. Mass Spectrom.* **2017**, *28*, 2686; b) K. Kulyk, O. Rebrov, M. H. Stockett, J. D. Alexander, H. Zettergren, H. T. Schmidt, R. D. Thomas, H. Cederquist, M. Larsson, *Int. J. Mass Spectrom.* **2015**, *388*, 59.
[35] D. A. Thomas, R. Chang, E. Mucha, M. Lettow, K. Greis, S. Gewinner, W. Schöllkopf, G. Meijer, G. von Helden, *Phys. Chem. Chem. Phys.* **2020**, *22*, 18400.
[36] a) W. F. Visser, N. M. Verhoeven-Duif, R. Ophoff, S. Bakker, L. W. Klomp, R. Berger, T. J. de Koning, *J. Chromatogr. A* **2011**, *1218*, 7130; b) S. Karakawa, K. Shimbo, N. Yamada, T. Mizukoshi, H. Miyano, M. Mita, W. Lindner, K. Hamase, *J. Pharm. Biomed. Anal.* **2015**, *115*, 123; c) K. Yoshikawa, M. Furuno, N. Tanaka, E. Fukusaki, *J. Biosci. Bioeng.* **2020**, *130*, 437.

Manuscript received: December 18, 2023
Revised manuscript received: February 23, 2024
Accepted manuscript online: February 28, 2024
Version of record online: ■■, ■■

RESEARCH ARTICLE

Chiral analytes from a microfluidic chip reactor are transferred to the gas phase where they form diastereomeric complexes with a volatile chiral selector, which are spectrally differentiated by cryogenic ion trap vibrational spectroscopy. The enantiomeric ratio is rapidly determined online with minimal sample consumption and with competitive accuracy.

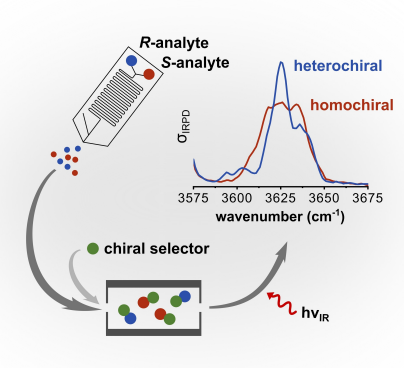

*S. Schmahl, F. Horn, Dr. J. Jin, H. Westphal, Prof. Dr. D. Belder, Prof. Dr. K. R. Asmis**